Cardiovascular Engineering and Technology, Vol. 10, No. 4, December 2019 *(© 2019)* pp. 553–567
https://doi.org/10.1007/s13239-019-00428-z

Optimization Framework for Patient-Specific Cardiac Modeling

JOSHUA MINEROFF,[1] ANDREW D. MCCULLOCH,[2] DAVID KRUMMEN,[3] BASKAR GANAPATHYSUBRAMANIAN,[1] and ADARSH KRISHNAMURTHY[1]

[1]Department of Mechanical Engineering, Iowa State University, Ames, IA, USA; [2]Bioengineering and Medicine, University of California, San Diego, La Jolla, CA, USA; and [3]Department of Medicine (Cardiology), University of California, San Diego, La Jolla, CA, USA

(Received 10 April 2019; accepted 5 August 2019; published online 17 September 2019)

Associate Editor Alison Marsden and Ajit P. Yoganathan oversaw the review of this article.

Abstract
Purpose—Patient-specific models of the heart can be used to improve the diagnosis of cardiac diseases, but practical application of these models can be impeded by the computational costs and numerical uncertainties of fitting mechanistic models to clinical measurements from individual patients. Reliable and efficient tuning of these models within clinically appropriate error bounds is a requirement for practical deployment in the time-constrained environment of the clinic.
Methods—We developed an optimization framework to tune parameters of patient-specific mechanistic models using routinely-acquired non-invasive patient data more efficiently than manual methods. We employ a hybrid particle swarm and pattern search optimization algorithm, but the framework can be readily adapted to use other optimization algorithms.
Results—We apply the proposed framework to tune full-cycle lumped parameter circulatory models using clinical data. We show that our framework can be easily adapted to optimize cross-species models by tuning the parameters of the same circulation model to four canine subjects.
Conclusions—This work will facilitate the use of biomechanics and circulatory cardiac models in both clinical and research environments by ameliorating the tedious process of manually fitting the parameters.

Keywords—Optimization, Cardiac biomechanics, Lumped-parameter circulation model, Patient-specific modeling.

INTRODUCTION

Physical models have been a foundational category of computer-based medical decision aids for at least 30 years[39] and advances in algorithms and computing power continue to improve the tractability of higher-fidelity analysis.[4] Patient-specific modeling (PSM) is the process of using clinical data to individualize computational models that integrate clinical data and use prior physiological knowledge and physicochemical constraints to make individualized predictions and decisions. PSM of cardiac mechanics and hemodynamics often relies on lumped parameter models of circulatory dynamics that often have too many adjustable parameters to identify uniquely from available clinical measurements alone. Similarly, certain parameters of constitutive laws for nonlinear anisotropic passive and active material properties of cardiovascular tissues can be adjusted to allow model predictions to match clinical measurements, but only if others are constrained by prior knowledge such as multi-axial *ex-vivo* tissue tests.

Existing approaches to fitting model parameters have used specialized tuning methods. More general tuning can allow non-experts in optimization a reasonable approach to tuning medium-dimensionality problems in their domain, ultimately leading to wider adoption of automated tuning methods. A universal framework can also be adapted by someone with expert knowledge of the model and algorithm to suit their workflow. The abstraction of the internals of such a 'black box' could then be compared to the internals of an ultrasound or CT system, which have long histories of successful employment in clinical settings.

In order to improve the objectivity of constrained parameter estimation and reduce the manual tuning required for PSM, we propose a new optimization-based framework to support the wider application of patient-specific physical models to the treatment of cardiovascular disease (CVD). We tested this framework using two examples: a hemodynamic lumped-parameter circulation model and a left ventricular (LV) passive finite-

Address correspondence to Adarsh Krishnamurthy, Department of Mechanical Engineering, Iowa State University, Ames, IA, USA. Electronic mail: mineroff@iastate.edu, amcculloch@ucsd.edu, baskarg@iastate.edu, and adarsh@iastate.edu

element model. The framework is used to determine the hemodynamic parameters of eight human patients using only limited non-invasive measurements to generate pressure–volume (P–V) loops of the different chambers of the heart. The finite-element model is used to determine the unloaded geometry and the cardiac tissue material parameters of four canine subjects based on data made available from a previous benchmark study,[42] followed by the circulation model to determine the hemodynamic parameters. This demonstrates the broad applicability of the proposed method in handling different mechanistic models in different species.

The main contributions of this work include the development of:

1. A framework to automatically tune biomechanics and circulatory cardiac models using patient-specific data with minimal user intervention.
2. A robust optimization formulation to fit parameters of full cardiac-cycle circulatory models, even with missing clinical data in certain patients.
3. A methodology that is applicable for different types of mechanistic models and enables automatic tuning of cross-species models.

This study shows that application of the proposed formal optimization methodology resulted in lower errors and variability than manual estimation performed on the same patients. The framework can facilitate the widespread use of patient-specific models by enabling model tuning using non-invasive data.

METHODS

Optimization Framework

Our framework (Fig. 1) is designed to perform parameter optimization to tune patient-specific computerized biophysical models to available data. The multi-modal, highly corrugated nature of these models makes it difficult to compute gradients and favored a derivative-free approach. We selected a hybrid particle swarm and pattern search solver to globally search the parameter space and support parallel model evaluation. Since model analysis is the primary computational expense for this class of problems, the potential overhead of a higher-level software package is insignificant.

Particle swarm optimization (PSO) is a heuristic method using a population of candidate solutions, referred to as particles.[38] Initially, these particles are distributed throughout the parameter space with a given location and 'velocity.' A step of the algorithm starts with the evaluation of the current parametric configuration of each particle. Then, the velocities of each particle are updated as a function of (1) its current velocity, (2) the best solution that it has found, and (3) the best solution any particle has found. The algorithm continues until a termination criteria is met, usually when a set number of iterations have passed without improving the objective value by a given tolerance. One of the primary benefits of PSO is its fast convergence in global search for traditionally difficult problems, but it is an expensive method for computing precise optima.

Pattern search is a direct search method (DS) involving the use of a scalable pattern, or mesh, to step through the parameter space from an initial location.[18] At each iteration, the mesh is centered at the current best point and parameter values at the surrounding mesh points are evaluated. The specific mesh pattern used polls a positive and negative perturbation of every parameter at each iteration. If an improvement is found, the mesh is re-centered at the new location and expanded to minimize the chances of convergence to a non-global minimum. If no improvement is found, the

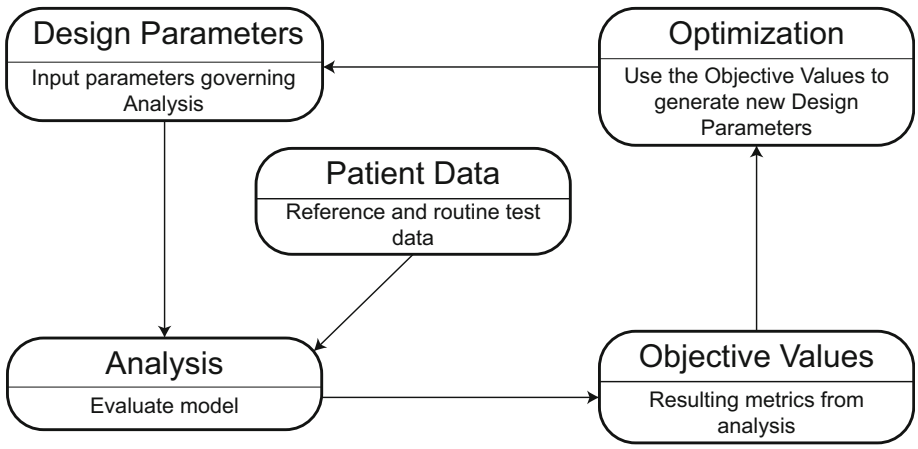

FIGURE 1. A flowchart of the general model tuning framework.

mesh is contracted to more precisely identify the local optimum. DS methods are highly influenced by initially assumed parameter values, but are one of the most efficient non-analytical methods for the identification of a precise solution.

The full hybrid algorithm we employed first searches the solution space using PSO to identify a likely global optima. Since PSO searches randomly but uniformly over the search space, there is a larger chance that it will encounter the global optimum's basin of attraction for non-convex problems. The trade-off is that PSO can typically be quite slow to converge to a precise optimum. Once a reasonable objective function tolerance was achieved, the resulting PSO solution was then used to initialize the DS method to more efficiently find a precise optimum. Using DS first would make convergence to a local optimum much more likely. The application of this is represented concretely in the canine ventricular inflation section—where we only use the DS method due to computational expense and suspected problem convexity.

This method differs from similar box-constrained methods like that used by Vaz and Vicente[41] in that we sequentially couple the two optimization solvers (i.e. PSO to termination first followed by DS to termination next), as opposed to using an alternatively coupled solver that switches between PSO and DS every iteration. It is generally impossible to prove that the true global optimum has been identified for non-analytical multi-modal problems, but in our experience, this approach converges to an acceptable result within the bounded parameter space for a majority of the runs. Secondly, PSO and DS can individually be expected to perform well on a wide-variety of problem classes.[30] Further implementation details can be found in Supplement A.

All optimization and analysis was run on a cluster with each node having two 2.6 GHz 8-Core Intel E5-2640 v3 processors and 128GB of RAM. The framework is implemented in MATLAB,[29] since it has multiple commercially-tested derivative-free solvers and is capable of integrating with most models, and will be made available after publication. The primary computational expense for the kind of optimization problems studied in this paper are the many model evaluations required. Both optimization methods used in our approach are well-suited to parallelization which can decrease the wall time of the optimization by allowing a larger pool of computational resources to be used than could be applied to a single evaluation. This is especially attractive with the increasing use of cloud computing. Parallelization was handled differently for each model and is further explained in each section.

Clinical Data

The eight human patients studied were male, aged (66 ± 11 years) with NYHA class III heart failure, dilated cardiomyopathy, and left bundle branch block (LBBB) were enrolled from the Veteran's Administration San Diego Healthcare System (San Diego, CA). Patients gave informed consent to participate in the human subject protocol approved by the institutional review board. All patients were part of a cardiac resynchronization therapy (CRT) study and were implanted with a biventricular pacemaker. Key cardiac measurements were recorded *via* echocardiogram, electrocardiogram (ECG), and routine diagnostic methods before pacemaker implantation; pressure data from cardiac catheterization was used for validation.

The heart rate (HR) was controlled during cardiac catheterization using RV pacing, just before pacemaker implantation, causing them to have the same HR value. Patient E was paced at a lower rate. The catheter pressure measurements are averaged over multiple beats obtained while pacing with breath-hold. The cuff pressure measurements were obtained at the same time as the echocardiographic measurements, two months before the pacemaker implantation. End diastolic volume (EDV) was obtained *via* Simpsons method from two views of the echocardiographic images. The timing of end-diastole was measured using the start of the QRS complex in the ECG.

Canine Subject Data

The canine simulations used four normal dog data provided by the STACOM 2014 LV Mechanics Challenge.[7] The data was acquired at the National Institute of Health, USA in collaboration with Johns Hopkins University[14] using high resolution cines, tagging, and *ex-vivo* diffusion tensor imaging (DTI).[42] Data acqui-

TABLE 1. Experimentally measured objectives for canine subjects studied in circulatory optimization.

Subject	$Pmax_{LV}$ (kPa)	EDV_{LV} (mL)
S1	13.6	30.3
S2	12.3	20.5
S3	10.3	24.5
S4	11.3	19.6

All subject models relied largely on reference data. $Pmax_{LV}$ peak left-ventricular pressure, EDV_{LV} left-ventricular end-diastolic volume.

sition was approved by local Institutional Review Boards and conducted in accordance with the "Guide for the Care and Use of Laboratory Animals".[19] *In-vivo* left ventricular pressures were also recorded during scanning (Table 1). Dogs were paced from the right atrium.

Circulation Model

CircAdapt[2] is a lumped-parameter model of the circulatory system (Fig. 2) implemented in MATLAB. It can be used to model the pressure and volume of the four chambers as a function of time for the complete cardiac cycle. We use CircAdapt to perform a closed-loop simulation of the patient-specific cardiovascular system, incorporating up to 11 values of non-invasively obtained patient data, and output one simulated cycle of blood flow. The potential data include HR, blood pressure (BP), and valve measurements (e.g. diameter and regurgitation) that can be obtained through ECG or echocardiogram (Table 3). Mean systemic blood flow, q, was derived from EDV and ESV.

CircAdapt has more parameters than can be feasibly tuned for a patient, so it is necessary to select a subset of model parameters for tuning (Table 2). Once the objective metrics were chosen, we were able to find the most directly-related parameters and that is the set of 9 that we used. Some specific parameters, e.g. L_{aorta}, were found to be necessary through early experimentation. The vector of these parameters is represented by $\mathbf{x}$. The length, N, of this vector is equal to the number of parameters in the optimization problem, which is 9 in this case.

The CircAdapt model is a system of ODEs that compute the hemodynamics of the heart and circulation. The cardiac part of the model is the so-called TriSeg model. The model is usually started with the default parameter values and any change to the parameter values take a few cycles for the circulation system to reach steady state. In order to better represent the steady state system of the circulation, we run several beats of the model after changing the parameters from the default values to the patient-specific values. To improve model stability to support large perturbations from parameters and data, adaptation from the default configuration was performed in three steps. Adaptive convergence methods could be applied to improve this approach. In addition, CircAdapt also has a different set of equations to adapt the patient-specific parameters to a patient who is at *rest*. So in order to best achieve the steady state *rest* condition of the circulation model (i.e. conditions in which the measurements were taken), we first run the model without any adaptation, achieve steady state, then run the *rest* adaptation, and again run without adaptation to achieve a new steady state after the adaptation process. The complete CircAdapt convergence protocol was to run 30 beats each of *Adapt0*, *AdaptRest*, and *Adapt0*.

Since we were modeling the baseline hemodynamics of LBBB patients, setting the delay between the left

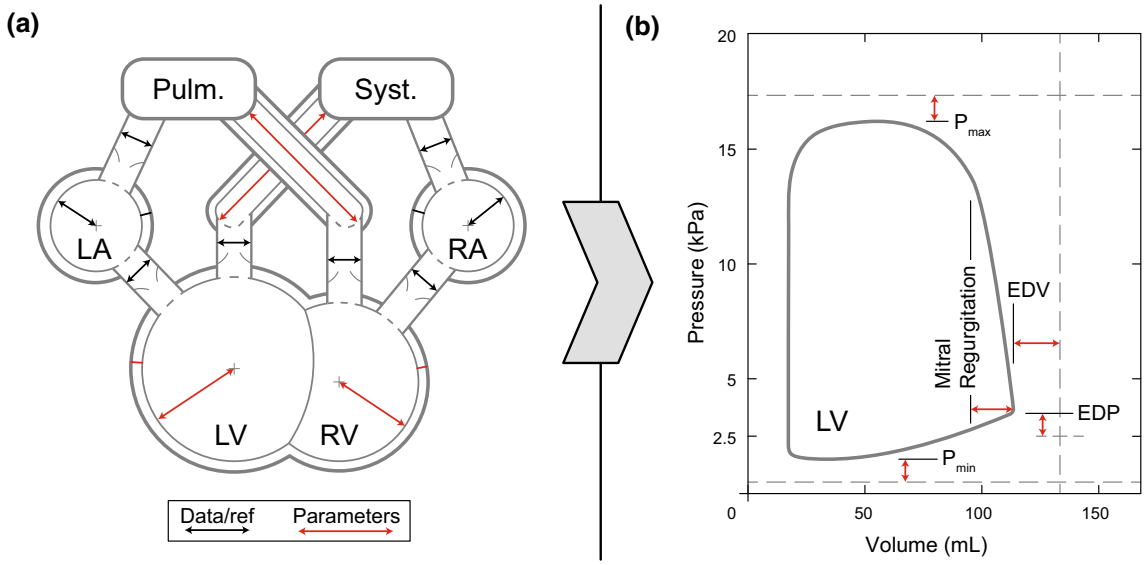

FIGURE 2. The geometric parameters and objective metrics used in the circulatory optimization. (a) A schematic of the CircAdapt model highlighting key geometric dimensions of major model components. A subset of the model values directly driven by patient-specific or reference data (Table 3) and the parameters used (Table 2) are both shown. (b) A typical simulated left ventricular (LV) pressure–volume loop showing all partial objective metrics. *Pulm.* pulmonary circulation, *Syst.* systemic circulation, *LA* left atrium, *RA* right atrium, *RV* right ventricle, *EDV* end-diastolic volume, *EDP* end-diastolic pressure.

TABLE 2. Parameters and bounds of the different optimization variables in x of the circulation model.

Variable	Description	Lower bound	Upper bound	Units	Reference
k_{MAP}	Scaling of mean arterial pressure initially calculated using the '33% formula'	0.8	1.2	–	36
$P\Delta_{pulm}$	Blood pressure head loss across the pulmonary system	0.5	1.5	kPa	32,45
L_{aorta}	Geometric scaling factor of effective length of aorta from CircAdapt reference configuration	0.5	1.5	–	
L_{pulm}	Geometric scaling factor of effective length of pulmonary artery from CircAdapt reference configuration	0.5	1.5	–	
k_{LV}	Geometric scaling factor of left ventricular midwall surface area from CircAdapt reference configuration	0.5	2	–	11
k_{RVrel}	Geometric scaling factor of right ventricular midwall surface area from CircAdapt reference configuration relative to left ventricle scaling	0.5	2	–	22
Sf_{act}	Maximum isometric active stress of myofibers	25	200	kPa	
Sf_{pas}	Passive stiffness of myofibers	10	30	kPa	
M_{leak}	Ratio of mitral valve leak area to open area	1e−6	0.2	–	46

TABLE 3. Experimentally measured and reference data for human patients studied in circulatory optimization.

Patient	*HR* (BPM)	*q* (mL/s)	*QRS* (s)	D_{aorta} (m)	D_{aortic} (m)	D_{pulm} (m)	D_{mitral} (m)	V_{wall} (m^3)	$Pmax_{LV}$ (kPa)	EDV_{LV} (mL)	*MRV* (mL)
Ref	*71*	*85e−6*	–	*25e−3*	*25e−3*	*26e−3*	*25e−3*	*213e−6*	*16.3*	*118*	–
A	70	80e−6	0.156	22e−3	34e−3	–	18e−3	260e−6	18.7	235	–
B	70	51e−6	0.148	34e−3	18e−3	–	16e−3	190e−6	14.7	177	15
C	70	100e−6	0.162	–	22e−3	18e−3	23e−3	270e−6	15.5	142	–
D	70	84e−6	0.130	–	24e−3	15e−3	23e−3	450e−6	20.1	289	30
E	60	45e−6	0.128	–	22e−3	–	42e−3	450e−6	13.1	257	–
F	70	55e−6	0.119	25e−3	25e−3	–	25e−3	309e−6	9.5	135	–
G	70	46e−6	0.140	36e−3	23e−3	–	16e−3	290e−6	6.7	198	–
H	70	56e−6	0.124	35e−3	21e−3	–	16e−3	237e−6	16.3	166	–

Reference values are given in italics.

The *ref* row describes the default values in CircAdapt. Missing measurements were substituted by appropriately scaling these values. *HR* heart rate, *q* mean systemic blood flow, *QRS* QRS complex duration, D_{aorta} diameter of aorta, D_{aortic} open diameter of aortic valve, D_{pulm} open diameter of pulmonary artery, D_{mitral} open diameter of mitral valve, V_{wall} ventricular wall volume, $Pmax_{LV}$ peak left-ventricular pressure, EDV_{LV} left-ventricular end-diastolic volume, *MRV* mitral regurgitant volume.

and right ventricular activation is important to get a good agreement with the measured data. In this respect, the QRS duration of each of the 8 patients were measured using ECG. In the CircAdapt model (specifically in the myofilament parameters), the QRS duration was used to set the delay in activation of the LV with respect to the RV activation time.

Primary model fit was assessed as a function of the relationships of simulated peak pressure (P_{max}, Eq. 1) and end-diastolic volume (EDV, Eq. 3) to measured patient values, with additional constraints that are enforced as penalties to the objective function. These penalties were based on (1) minimum LV pressure (P_{min}: 0.5 kPa, Eq. 2), (2) LV end-diastolic pressure (EDP: 2.5-4 kPa, Eq. 4), and (3) mitral regurgitant volume (MRV, Eq. 5).

The component weights of the objective function (Eq. 6) were selected to prioritize those with greater certainty and reduce those relying on assumptions from reference data. The contribution of constraints on P_{min} and EDP were weighted the least, as they were not derived from patient data, while P_{max} was weighted highly, as it was measured most directly. These weights were also informed by the resulting ranges of each component; for example, the P_{min} error was typically very small so the corresponding term did not contribute heavily to the objective even with the larger coefficient of 0.75. Additionally, positive P_{max} and EDV model error were penalized by a factor of 2; this reduced the likelihood that one value was unreasonably increased to marginally improve the other or as a result of possible measurement overestimation.[26,35] This helped to constrain the P–V loops within the physiological domain. If no MRV patient data was available, then a healthy reference value of 30 mL was used as an upper bound; 3 mL was used for the canine subjects. Our framework could be easily adapted to use other objective functions motivated by biomechanical principles or physiology (e.g. Heusinkveld *et al.*[16]).

$$y_{Pmax}(\mathbf{x}) = \begin{cases} \left(\frac{Pmax(\mathbf{x}) - \mathbf{Pmax_{data}}}{Pmax_{data}}\right)^2, & \text{if } Pmax(\mathbf{x}) \leq \mathbf{Pmax_{data}} \\ 2 * \left(\frac{Pmax(\mathbf{x}) - \mathbf{Pmax_{data}}}{Pmax_{data}}\right)^2, & \text{if } Pmax(\mathbf{x}) > \mathbf{Pmax_{data}} \end{cases} \quad (1)$$

$$g_{Pmin}(\mathbf{x}) = \left(\frac{Pmin(\mathbf{x}) - \mathbf{Pmin_{ref}}}{Pmax_{data} - Pmin_{ref}}\right)^2, \quad \text{if } Pmin(\mathbf{x}) > \mathbf{Pmin_{ref}} \quad (2)$$

$$y_{EDV}(\mathbf{x}) = \begin{cases} \left(\frac{EDV(\mathbf{x}) - \mathbf{EDV_{data}}}{EDV_{data}}\right)^2, & \text{if } EDV(\mathbf{x}) \leq \mathbf{EDV_{data}} \\ 2 * \left(\frac{EDV(\mathbf{x}) - \mathbf{EDV_{data}}}{EDV_{data}}\right)^2, & \text{if } EDV(\mathbf{x}) > \mathbf{EDV_{data}} \end{cases} \quad (3)$$

$$g_{EDP}(\mathbf{x}) = \begin{cases} \left(\frac{EDP(\mathbf{x}) - \mathbf{EDP_{refmin}}}{Pmax_{data} - Pmin_{ref}}\right)^2, & \text{if } EDP(\mathbf{x}) \leq \mathbf{EDP_{refmin}} \\ \left(\frac{EDP(\mathbf{x}) - \mathbf{EDP_{refmax}}}{Pmax_{data} - Pmin_{ref}}\right)^2, & \text{if } EDP(\mathbf{x}) > \mathbf{EDP_{refmax}} \end{cases} \quad (4)$$

$$g_{MRV}(\mathbf{x}) = \begin{cases} \left(\frac{MRV(\mathbf{x}) - \mathbf{MRV_{data}}}{MR_{data}}\right)^2, & \text{if } MRV_{data} \neq \\ \left(\frac{MRV(\mathbf{x}) - \mathbf{MRV_{ref}}}{MR_{ref}}\right)^2, & \text{if } MRV_{data} = \text{ and } MRV(\mathbf{x}) > \mathbf{MRV_{ref}} \end{cases} \quad (5)$$

$$\begin{aligned} f(\mathbf{x}) = & 0.8 * y_{Pmax}(\mathbf{x}) + \mathbf{0.2} * \mathbf{y_{EDV}}(\mathbf{x}) \\ & + 0.75 * g_{Pmin}(\mathbf{x}) + \mathbf{0.75} * \mathbf{g_{EDP}}(\mathbf{x}) \\ & + 0.15 * g_{MRV}(\mathbf{x}) \end{aligned} \quad (6)$$

The goal of the optimization problem is to find $\mathbf{x}$ such that $f(\mathbf{x})$ (Eq. 6) is minimized, subject to the parameter bounds on $\mathbf{x}$ listed in Table 2.

This optimization formulation was used to generate CircAdapt models for eight human patients and four canine subjects. This resulted in 45 (5N) evaluations for each PSO iteration and 18 (2N) iterations for each DS iteration. Each optimization was run in a MATLAB environment on one 16-core node, allowing for 16 parallel single-threaded evaluations. Repeated parameter configurations used the initial result for improved efficiency.

Finite Element Model of Canine Left Ventricular Inflation

In this section, we show the applicability of our optimization framework to identify the material parameters and unloaded geometry of a finite element ventricular model.

The canine data was the same as the ones used for the circulation model optimization. Additional processed data included mesh point clouds and binary masks defining the LV geometry and muscle fiber orientations derived from *ex vivo* diffusion tensor MRI. The geometries only reflect the location of the epicardial and endocardial surfaces; they do not encode material point displacements. The finite element geometry for the dog models were reconstructed using the methods outlined in Krishnamurthy *et al.*[24]

We use a finite-element model of the canine LV to determine its unloaded state and personalized material parameters of the cardiac tissue. An analysis-suitable LV mesh is constructed from an MRI scan of the subject or patient heart at end-diastole. However, since this mesh is measured at the loaded (pressurized) state, an unloaded (unpressurized) mesh state needs to be determined along with the properties of the passive Ogden-Holzapfel material model.[17]

The unloaded mesh is obtained through an iterative inflation-deflation process based on the methods of Bols *et al.*[6] and Sellier.[37] We first assume an initial unloaded LV geometry that is identical to the MRI mesh, and passively inflate it to the measured EDP. Then the deformation gradient between the loaded and MRI mesh is inversely applied to the unloaded geometry. This process is repeated until the interior volume of the loaded mesh and MRI mesh converge to within 3%.[23]

$$\psi = \frac{a}{2b} e^{b(I_1 - 3)} + \frac{a_f}{2b_f}\left(e^{b_f(I_{4f} - 1)} - 1\right) \quad (7)$$

Four material model parameters (a, b, a_f, and b_f, Table 6) are used to represent patient-specific material properties in a simplified form of the Ogden-Holzapfel strain energy function (Eq. 7). Correctness of the material parameters is determined by the conformation of the resulting inflated ventricle to the reference end-diastolic P–V relationship (EDPVR) described by Klotz[21]; a similar approach was used by Augustin[3] and Nasopoulou *et al.*[31] The EDPVR formulation uses the sole original end-diastolic pressure (EDP) and volume (EDV) data point to describe the entire EDPVR as a

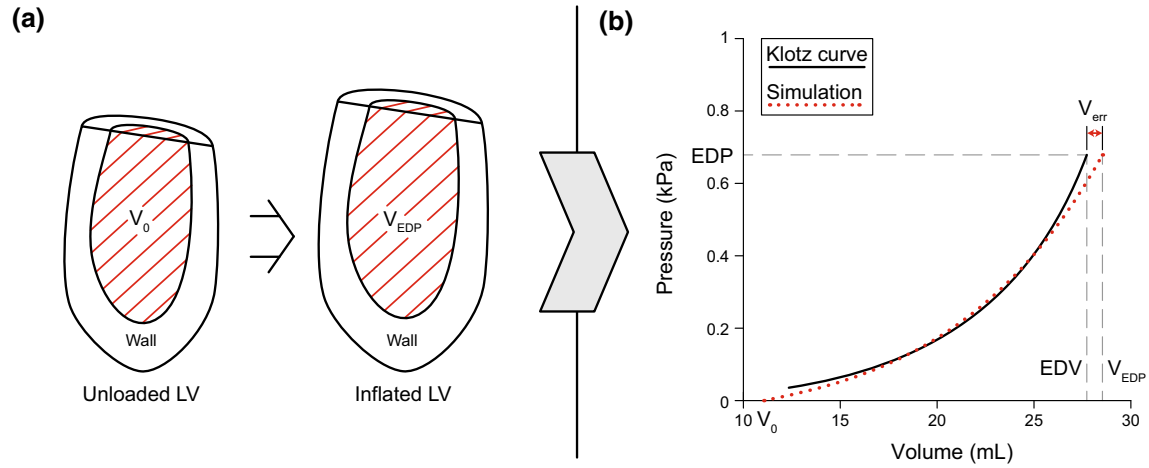

FIGURE 3. A representative example of both mesh states of the finite-element optimization and the resulting EDPVR curve. (a) A converged unloaded and inflated mesh from the simulation showing the change in ventricular shape and volume. (b) A comparison of the precomputed Klotz curve[21] and simulated pressure–volume curve. *EDPVR* end-diastolic pressure–volume relationship.

function (Eq. 8) with patient-specific values α and β. The calculation of those values uses some experimentally-determined constants and is described in detail in that paper. Here, i denotes discrete sampling locations along the EDPVR. The least squares error is then calculated between this curve and the complete set of data captured during the simulated inflation (Fig. 3).

$$EDP_i = \alpha * EDV_i^{\beta} \tag{8}$$

The optimized material parameter values are those that minimize this error (Eq. 9). The first term of this summation describes the pressure at a given step in the simulation while the second term describes the Klotz-predicted pressure at the corresponding volume. We used four meshes generated from canine subjects to demonstrate the approach. Note that the objective components are not normalized like in Eq. 6—as there is only one target. In contrast, for the CircAdapt model it was necessary to balance the fit of EDV and P_{max} with each other and the other listed criteria.

$$f(x) = \sum_{i=1}^{n} (P_i(x) - \alpha(x) EDV_i(x)^{\beta(x)})^2 \tag{9}$$

Evaluation of this model is significantly more expensive than the circulation model, and is therefore optimized using only the more computationally efficient DS portion of the optimization framework. This shows how the exact implementation of the framework can be easily adapted to different problems. The MATLAB-based DS optimization framework generated eight (2N) parameter configurations for each mesh iteration of the optimization algorithm. The evaluation of these was handled *via* a queue managed by GNU Parallel[40] to run up to eight evaluations in parallel across four nodes. A bash script was used to control the inflation/deflation cycle until the model had converged. Each simulation was performed using Continuity 6.4,[12] a Python-based multi-scale FEA and modeling tool developed by the UCSD Cardiac Mechanics Research Group, in parallel across eight cores. This approach is highly scalable with a minimal amount of overhead.

RESULTS

Circulation Model Results

Patient-specific circulatory models were tuned for the eight human subjects using CircAdapt with the presented optimization framework to determine parameter values (Table 4). The pressure error for the eight patients had a max of 0.53% and a mean of 0.15%. Volume error had a max of 6.71% and a mean of 1.26%. Only the models for patients A and E exceeded the reference minimum pressure value of 1 kPa, with patient E having the highest value of 1.18 kPa, but all models had acceptable EDP values within 18% of the 2.5 kPa reference value. Mitral regurgitant volume was within 1.3 mL of the measured value for two of the patients where data was available (B and D), and within the (< 30 mL) healthy range for patients that did not have that data. The low measured regurgitant volume (5 mL) of patient E was not able to be satisfied, contributing significantly (30%) to the objective value.

The tuned models for patients A and E had significantly higher optimized objective values than the other six patients (0.21e−3 and 1.23e−3 respectively, compared to the overall median of 6.4e−8), primarily from EDV error. The model for patient F was the best optimization result, with an objective value of 6e−9.

TABLE 4. Optimized parameters and results of human patients and canine subjects studied in circulatory optimization.

Pat/ Sub	k_{MAP} –	$P\Delta_{pulm}$ (kPa)	L_{aorta} –	L_{pulm} –	k_{LV} –	k_{RVrel} –	Sf_{act} (kPa)	Sf_{pas} (kPa)	M_{leak} –	Obj 1e−3	$Pmax_{err}$ %	EDV_{err} %
Ref	*1*	*1.5*	*1*	*1*	*1*	*1*	*120*	*4.0*	*1e−6*	–	–	–
A	1.15	**0.50**	1.31	0.86	1.57	**0.50**	**200**	**10.0**	7.1e−2	0.21	−0.53	−2.39
B	1.04	0.77	0.68	1.23	1.30	0.53	142	22.9	4.7e−2	0.00	−0.02	−0.00
C	1.18	1.24	1.46	0.54	1.19	0.79	171	24.4	4.5e−3	0.00	0.01	0.00
D	1.15	**0.50**	1.49	1.46	1.68	**0.50**	198	10.0	4.7e−2	0.02	−0.03	−0.95
E	0.99	0.50	1.26	0.51	1.48	0.70	158	22.2	8.7e−4	1.23	−0.50	−6.71
F	0.92	0.81	1.00	1.35	1.33	0.63	200	19.4	2.2e−2	0.00	−0.01	−0.01
G	1.04	1.14	0.53	0.64	1.55	0.64	149	24.7	5.4e−2	0.00	0.02	0.00
H	0.95	1.22	1.30	0.91	1.29	1.08	193	29.3	2.9e−2	0.00	−0.03	0.00
μ	*1.05*	*0.84*	*1.13*	*0.94*	*1.42*	*0.67*	*176*	*20.3*	*0.03*	*0.18*	*0.15*	*1.26*
σ	±0.10	±0.33	±0.36	±0.37	±0.17	±0.19	±24	±7.0	±0.02	±0.43	±0.23	±2.36
S1	1.06	**1.50**	0.92	0.53	1.28	1.30	194	10.1	**1e−6**	0.22	−0.45	0.05
S2	1.06	1.30	1.48	1.49	1.18	0.53	171	**10**	1.3e−6	0.10	−0.14	−0.33
S3	1.13	1.42	1.25	1.29	1.28	0.53	153	28.7	1.3e−3	7.48	0.02	−0.27
S4	1.11	1.03	0.50	1.50	1.17	0.71	115	29.7	**1e−6**	0.00	0.14	−0.08
μ	*1.09*	*1.31*	*1.3*	*1.2*	*1.23*	*0.77*	*158*	*19.6*	*3.3e−4*	*1.95*	*0.19*	*0.18*
σ	±0.04	±0.21	±0.27	±0.46	±0.06	±0.37	±33	±11.1	*±6.5e−4*	±3.69	±0.18	±0.14

Reference values are given in italics.
The *ref* row describes the default values in CircAdapt. Bounded optimal parameter values are bolded. Explanation of variables can be found in Table 2. Patient-specific data and target metrics can be found in Table 3.

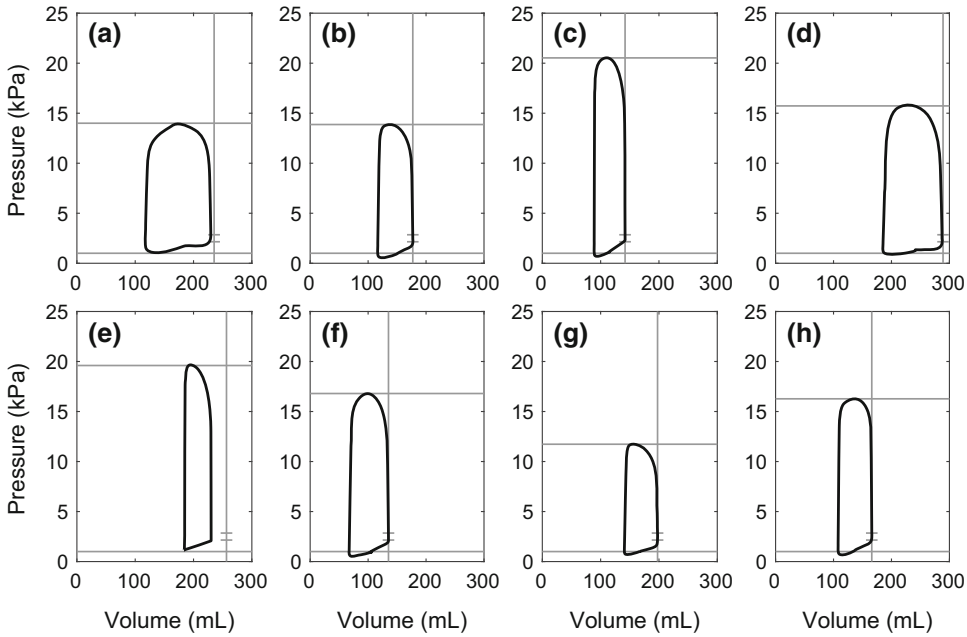

FIGURE 4. Left ventricular pressure–volume loops for the eight human patients. Light gray lines show the fitting targets. The small hash marks around 2.5 kPa represent the unpenalized EDP range.

Parameter values were not consistently bounded and were typically distributed through the allowable range. None of the LV P–V loops from each of the tuned models (Fig. 4) have any obvious artifacts that would signify errors in CircAdapt model convergence.

Since PSO is stochastic, solution stability is an obvious concern. For each of the presented patients, the algorithm was run multiple times and resulted in similar objective values and constraint violations between runs—which is expected given that they are small to begin with. Additionally, the parameter values did not vary significantly (less than 10%) implying that the problem was not overparameterized.

CircAdapt models were also tuned for four canine subjects (Table 4), generating a set of P–V loops (Fig. 5). The objective values for these models were

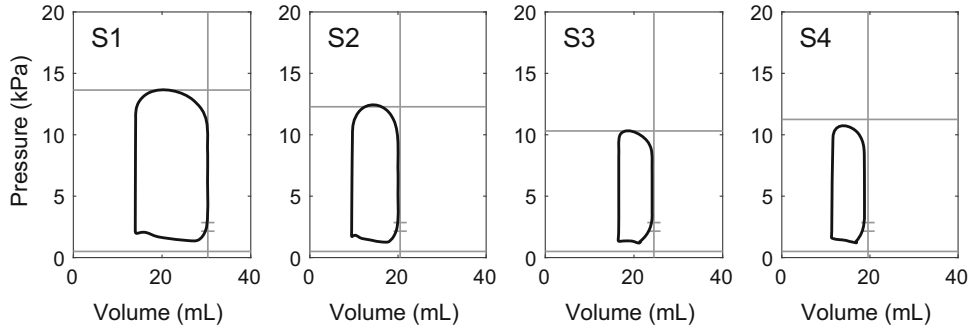

FIGURE 5. Left ventricular pressure–volume loops for the four canine subjects. Light gray lines show the fitting targets. The small hash marks around 2.5 kPa represent the unpenalized EDP range.

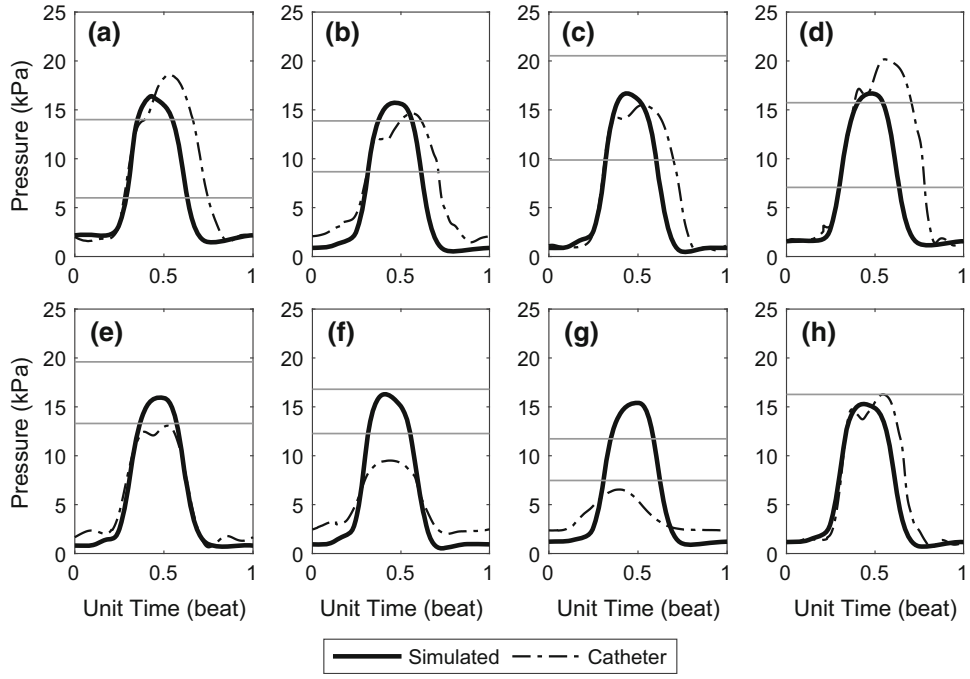

FIGURE 6. Validation of the simulated left ventricular pressure curves for the eight human patients with catheter data after tuning the optimized results with the average *MAP* and Sf_{act}. Gray lines show cuff measurement systolic and diastolic pressures—only catheter pressure was available as the reference for Patient H.

higher on average than the human patients (1.95e−3 vs. 1.8e−4). The primary source of errors varied across subjects, with S1 being most affected by P_{max} and S3 being most affected by EDP and P_{min}.

The average time to solution was 29 h, with a range of 25–40 h. The average number of model evaluations was 3875, ranging from 2257 to 5454; 8% of these were repeat configurations where the optimizer reevaluated a specific set of parameters, but returned the previously logged solution instead of rerunning the CircAdapt model.

Both sets of circulatory results were validated by calculating the root-mean-square error (RMSE) between the simulated pressure curves and the left ventricular catheter data that was available for the eight patients. The result highlights a potential downside of only using non-invasive measurements, because systolic cuff pressure data for the studied patients differed from peak LV catheter pressure by an average of 41%. Substituting the LV catheter pressure for cuff pressure as the optimization input reduced RMSE by an average of 31%; patient E error decreased by 69% (Fig. 13). It must be noted that catheter measurements are not routinely performed on heart failure patients. We tried several different approaches to get an effective simulated pressure time-course in the absence of reliable, invasive BP data; we discuss these approaches in detail in Supplement B. The approach that gave the best result was to optimize the patients using the cuff systolic pressure first and then replacing the MAP and

Sf_{act} for all patients with an average value (Fig. 6). This method reduced the RMSE error for most patients except for patient G and H (Table 5) and the authors expect that this is due to some uniqueness of the studied population relative to the general healthy population initially used to create the CircAdapt model. If this model were to be clinically applied, it would be appropriate to compute more accurate reference starting values for different classes of diseased patients. That reasonable results were obtained without more tailored starting values supports the stability of the approach.

Since cuff pressure was not available for the canine subjects, catheter data was used as a direct optimization input. This led to a lower average RMSE than for the non-invasive human patient results (1.6 kPa vs. 3.12 kPa, Fig. 7). One of the largest contributors to the calculated RMSE values was inaccuracy in the total time of cardiac tissue activation. While the activation time for normal patients can be measured directly from QRS, we cannot directly subtract the timing delay between the LV and RV for the heart failure patients studied. This value was not a parameter in the optimization, since there was no available patient data to evaluate it against, and thus remained at the typical reference value. Table 5 shows the RMSE values for each subject and each patient when optimized with cuff and catheter pressure (Table 6).

TABLE 5. RMSE between both human and canine model and catheter data when either peak systolic cuff (with or without using the mean values of *MAP* and Sf_{act}) or catheter pressure is used as an optimization target.

Subject/patient	Cuff (kPa)	Mean (kPa)	Cath (kPa)
A	4.07	2.90	2.41
B	2.66	2.57	2.75
C	2.85	2.53	2.78
D	4.59	4.08	3.28
E	3.11	1.53	0.97
F	3.48	3.29	1.43
G	2.79	4.44	1.39
H	1.42	1.55	1.42
S1	–	–	1.30
S2	–	–	1.41
S3	–	–	1.11
S4	–	–	2.72

FEA Model Results

Material properties for four canine subjects were fitted using a left-ventricular passive inflation simulation in Continuity (Table 7). The optimized values for all subjects were notably dissimilar from the reference values. S1 had much different values than the other subjects, likely caused by its significantly greater chamber volume. The average least squares error was

TABLE 6. Parameters and bounds of coefficients of x in Eq. 9.

	a (kPa)	a_f (kPa)	b –	b_f –
Upper bound	50	50	50	50
Reference	1.5	15	8	15
Lower bound	0.01	0.01	0.01	0.01

TABLE 7. Optimized coefficients from Eq. 9 and Klotz curve[21] fit for each canine subject

Subject	a (kPa)	a_f (kPa)	b –	b_f –	Objective –
Ref	*1.5*	*15*	*8*	*15*	–
S1	1.6	5.1	7.3	4.5	0.30
S2	0.1	11.1	4	14.3	0.22
S3	0.3	6.8	4.3	12.7	0.09
S4	0.4	4.8	4.5	43.5	0.21

Reference values are given in italics.

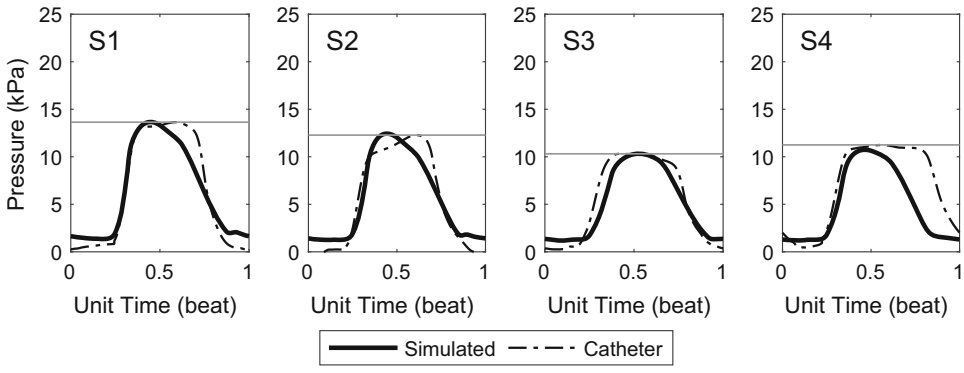

FIGURE 7. Validation of the simulated left ventricular pressure curves for the the four canine subjects with catheterized *in-vivo* pressure data. Gray line shows reference catheter pressure.

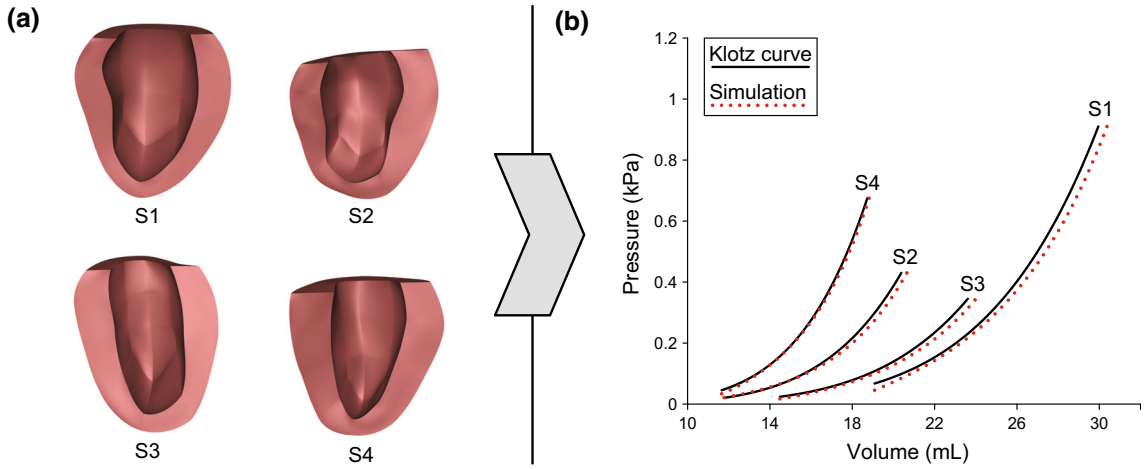

FIGURE 8. Results from simulated inflations of four canine left ventricles. (a) The final unloaded meshes. (b) Comparison of the optimized simulated pressure–volume curves to the Klotz curves.[21]

0.21, ranging from 0.09 to 0.30. Figure 8 shows the resulting unloaded meshes and EDPVR curves for all four subjects.

The largest impediment to fit was the allowed EDV convergence error for the estimation of the undeformed ventricle geometry. The average solution took 76 h with 1277 evaluations, each requiring 2–3 inflation deflation iterations; however the number of required unique evaluations varied widely between 374 and 3092, with repeat configurations used the previously logged result for efficiency.

DISCUSSION

Our results showed that the proposed optimization-based tuning framework avoids many of the issues inherent to manual tuning. Highly sophisticated models exist for many biophysical cardiac phenomena,[8,10,20,34,43] which require tuning of circulatory models. Circulatory models were tuned for individuals with widely-varied parameters, but acceptable solutions were found for all of them.

It would be very time-consuming and tedious to manually tune these models from a standard set of assumed parameter values in each case without considerable experience. The manual process also does not ensure repeatability of the parameter results. Evaluation of the manual tuning performed by Krishnamurthy *et al.*[25] on CircAdapt models of the same patients used in this study resulted in an average objective of 2.42e−3, 97% higher than even the worst result from our method; pressure was the largest error contributor. In addition, the manual process was significantly slower, with each patient requiring up to 4 days of manual tuning. Our optimized parameter values were also very different between individuals, suggesting that immediate local optima were avoided. We demonstrated the seamless integration of idealized reference values with patient-specific data, thereby accounting for missing data.

Most previous applications of optimization to circulatory model parameter fitting have used a localized or gradient-based approach; however, derivative-free and heuristic methods are more suitable for complex, multi-modal models where gradient-evaluation is expensive and there are many local optima that confuse the solver. Neal and Bassingthwaighte[33] used the Nelder-Mead Simplex algorithm (NMS) to tune two open-loop models of hemorrhage in porcine subjects, while Lim *et al.*[27] applied NMS to model an implantable rotary blood pump under various operating conditions. Ellwein *et al.*[13] used the gradient-based Levenberg-Marquardt algorithm to fit a lumped-parameter model of congestive heart failure. Balaban *et al.*[5] investigated the application of local optimizers with the multi-start method to further improve robustness and confidence in the optimized result. In this work, we demonstrate an efficient and reliable algorithm for optimizing hemodynamic models that can work for a wide variety of patients.

Automated model tuning supports wider application without the need for expensive manual tuning. Wang *et al.*[42] tuned passive LV material properties from MRI data using automatically-oriented myocardial fibers. Chabiniok *et al.*[9] the affect of varying geometric subdivisions on tissue contractility tuning for a porcine subject with infarct. Marchesseau *et al.*[28] used Unscented Transform to fit ventricular volume curves. Xi *et al.*[44] tuned diastolic material parameters by iterating hierarchical parameter sweeps. Hadjicharalambous *et al.*[15] tuned passive myocardial stiff-

ness with parameter sweeps. Our proposed framework allows non-experts in optimization a reasonable approach to tuning medium-dimensionality problems in their domain, ultimately leading to wider adoption of automated tuning methods.

One of the main insights that we obtained during implementation of the framework is that the objective function for the circulation model optimization had to be carefully selected. Generally, a well-formulated objective function will be smooth and accurately represent the desired trade-offs used to compare multiple solutions. Objective function selection is also typically an iterative process. An objective function including Pmax and EDV alone was not complete enough to obtain consistent optimization results. Without the addition of the other penalties, primarily from reference values, the resulting P–V loops were highly unrealistic in both shape and position. We also found that an appropriate QRS duration value was vital to avoid model artifacts caused by incorrect fill timing.

In support of our hybrid global approach, early experimentation with local optimizers produced poor results when applied to the CircAdapt model; this shows that some of the previous methods in the literature, such as NMS and Levenberg-Marquardt, may not be appropriate for certain patient-specific parameters in our optimization. Generally, local optimizers that are heavily influenced by initial assumptions offer improved convergence and precision; however, they can also increase the likelihood of issues due to sensitive parameters common in PSM which can easily be initialized in a non-global basin-of-attraction. These issues are especially common with constrained, over-parameterized models. The benefit of an initial search using heuristic global optimizers (like PSO) is that they do a good job of randomly sampling the physiologically-bounded space. This increases the probability that the optimal solution obtained is robust.

A key enabler in successfully optimizing overparameterized models is the correlation of the model parameters with physiologically relevant measurements. CircAdapt is a good example of such a model, where the model is parameterized using physically measurable quantities such as dimensions and flow rates. It is straightforward to set the appropriate parameter constraints for such a model, which in turn increases the probability that the optimization finds a physiologically feasible solution within the parameter bounds.

Though the proposed framework addressed many of the issues currently impeding the use of patient-specific cardiovascular models, there are still some key limitations to its application. The first is that the use of noninvasive data imposes limitations on accuracy and data acquisition. However, requiring invasive procedures reduces the value of the framework as compared to more traditional explorative methodologies. The most efficient response is to determine the data sources which are most sensitive and justify the most effort to capture accurately. UQ can also be used to identify necessary parameters or variables that are difficult to measure but do not explain much of the patient variance in model outputs, so they can be replaced by published population means for the clinical cohort under consideration. Krishnamurthy *et al.*[25] discusses patient-specific and population-averaged data use in patient-specific cardiac models in more detail.

In the circulatory optimization, k_{MAP}, Sf_{act}, and k_{LV} were the most sensitive parameters; all had mean-normalized standard deviations less than half the value of any other parameter. The values of these parameters are strongly correlated with P_{max} and EDV, which is not surprising as those metrics were most heavily weighted in the objective, meaning that the accuracy of those reference measurements will have a large effect on the results of the optimization. While myofiber stress increases as heart failure progresses—increased left ventricular diastolic pressure, increased left ventricular diameter, and myocardial thinning all contribute to increased myofiber stress—the parameters of active contractile stress development will be lower than for healthy subjects. Thus, the precise relationship between these factors is uncertain, and is therefore difficult to model, especially using a lumped-parameter model such as CircAdapt. One way to mitigate this measurement and model uncertainty would be to obtain cheap, but non-routine, measurements for patient P–V loop validation, such as echocardiographic volume at key points in the cardiac cycle.

We found that non-invasive measures of P_{max} were especially unreliable, and this has also been documented in the literature.[36] Obtaining pressure through catheterization is currently ideal for data reliability, but improvements in non-invasive measurement methods are necessary to enable the broader application of PSM. Along with the approach of averaging MAP and Sf_{act} discussed in the Results section, we also tried using diastolic cuff pressure as a reference for aortic diastolic pressure. However, none of these methods had a lower RMSE compared to the catheterized pressure measurements. These results can be found in Supplement B.

One valuable future development would be the coupling of the optimization of the FEA and CircAdapt models. The reason that was not done here is that CircAdapt and the FEA model use substantial different material models. While the CircAdapt model used a single exponential Fung-type model, the FEA model used the more recent Holzapfel and Ogden[17] model with multiple exponential terms. The Holzapfel

and Ogden[17] model allows us to better match the measured EDPVR than the single exponential model. Please refer to Aguado-Sierra *et al.*[1] for more details about the differences in the model. A possible option was to correlate the parameters of the two models. However, with only the 4 canine subjects, there was not enough data to build a reliable correlation between the two.

Another limitation is that it is generally impossible to prove that a global optimum has been found for non-convex non-analytical problems, so there is always the potential for a slightly better tuned result. It is also still necessary that an appropriate objective function be manually constructed to evaluate model fit, which can often be surprisingly difficult. This problem decreases in significance as the specific application of a model becomes more widespread; in such cases a ''state-of-the-art'' objective function and parameter bounds can be shared among researchers and clinicians without requiring local expertise.

The optimized canine material parameters in the FEA model all converged to apparently reasonable values with the initially-assumed loose bounds, suggesting that typical material parameters give relatively good results for a wide variety of individuals or that it is a convex problem. However, with the more complete orthotropic material model and complex geometries, the solution may well not be convex.[31]

For this work, the methodology was tuned for robustness over efficiency. With the large model perturbations required during the optimization, this meant that convergence of each CircAdapt model took up to 15 min. However, based on past experience we expect significant speedup to be possible—including potential conversion of the model to C++—in future work.

In summary, this framework can facilitate the widespread use of patient-specific or subject-specific models by enabling tuning from non-invasive data. The optimization methods employed are resource efficient and easily scalable to the needs and computational capacity of the application. Using an optimization framework, the information learned in the medical community can be easily and reliably distributed, making it relatively easy to tune a new patient model in a clinical environment compared with current manual methods. Finally, the framework is also usable in a research setting, where a major concern in cross-species research is maintaining a consistent protocol. By tuning both human and canine circulatory models with no modifications to the implementation besides reference parameter values we demonstrate that this concern can be naturally addressed. This work can be used in cross-species research and contribute to improved treatment of CVD.

ELECTRONIC SUPPLEMENTARY MATERIAL

The online version of this article (https://doi.org/10.1007/s13239-019-00428-z) contains supplementary material, which is available to authorized users.

FUNDING

This research was supported in part by the National Biomedical Computation Resource, NIH Grant 8 P41 GM103426-21 (Amaro and McCulloch), by the UC Center for Accelerated Innovation under NIH Grant 4 U54 HL11-9893, NIH Grant 1 R01 HL131753 (Segars, Krishnamurthy, McCulloch), by NSF Grant 1750865 (Krishnamurthy), and by the Joseph C. and Elizabeth A. Anderlik Professorship at Iowa State University (Mineroff). We would also like to show our gratitude to Dr. Judy Vance at Iowa State University for her extraordinary support.

CONFLICT OF INTEREST

Andrew D. McCulloch is a co-founder, equity holders and scientific advisory board member of Insilicomed Inc. and Vektor Medical, licensees of UCSD software used in this research. This relationship has been disclosed to the University of California San Diego and is overseen by an independent conflict of interest management subcommittee appointed by the university. Joshua Mineroff, David Krummen, Baskar Ganapathysubramanian, and Adarsh Krishnamurthy have declared that no competing interests exist.

ETHICAL APPROVAL

All applicable international, national, and/or institutional guidelines for the care and use of animals were followed. All procedures performed in studies involving human participants were in accordance with the ethical standards of the institutional and/or national research committee and with the 1964 Helsinki declaration and its later amendments or comparable ethical standards.

INFORMED CONSENT

Informed consent was obtained from all individual participants included in the study.

REFERENCES

[1]Aguado-Sierra J., A. Krishnamurthy, C. Villongco, J. Chuang, E. Howard, M. J. Gonzales, J. Omens, D. E.

Krummen, S. Narayan, R. C. P. Kerckhoffs, and A. D. McCulloch. Patient-specific modeling of dyssynchronous heart failure: a case study. *Prog. Biophys. Mol. Biol.* 107(1):147–155, 2011.

[2]Arts, T., T. Delhaas, P. Bovendeerd, X. Verbeek, and F. W. Prinzen. Adaptation to mechanical load determines shape and properties of heart and circulation: the CircAdapt model. *Am. J. Physiol.* 288:H1943–H1954, 2005.

[3]Augustin, C. M., A. Crozier, A. Neic, Prassl AJ, Karabelas E, Ferreira da Silva T, Fernandes JF, Campos F, Kuehne T, and G. Plank. Patient-specific modeling of left ventricular electromechanics as a driver for haemodynamic analysis. *Europace* 18:iv121–iv129, 2016.

[4]Baillargeon, B., N. Rebelo, D. D. Fox, R. L. Taylor, and E. Kuhl. The Living Heart Project: a robust and integrative simulator for human heart function. *Eur. J. Mech.* 48:38–47, 2014.

[5]Balaban, G., M. S. Alnæs, J. Sundnes, and M. E. Rognes. Adjoint multi-start-based estimation of cardiac hyperelastic material parameters using shear data. *Biomech. Model. Mechanobiol.* 15(6), 1509–1521, 2016.

[6]Bols, J., J. Degroote, B. Trachet, B. Verhegghe, P. Segers, and J. Vierendeels. A computational method to assess the in vivo stresses and unloaded configuration of patient-specific blood vessels. *J. Comput. Appl. Math.* 246:10–17, 2013.

[7]Camara, O., T. Mansi, M. Pop, K. Rhode, M. Sermesant, and A. Young (eds). Statistical Atlases and Computational Models of the Heart: Imaging and Modelling Challenges. New York: Springer, 2014.

[8]Carapella, V., S. A. Niederer, P. Lamata, M. J. Bishop, J. E. Schneider, P. Kohl, and V. Grau. Images as drivers of progress in cardiac computational modelling. *Prog. Biophys. Mol. Biol.* 115:198–212, 2014.

[9]Chabiniok, R., P. Moireau, P. F. Lesault, A. Rahmouni, J. F. Deux, and D. Chapelle. Estimation of tissue contractility from cardiac cine-MRI using a biomechanical heart model. *Biomech. Model. Mechanobiol.* 11(5), 609–630, 2012.

[10]Chabiniok, R., V. Y. Wang, M. Hadjicharalambous, L. Asner, J. Lee, M. Sermesant, E. Kuhl, A. A. Young, P. Moireau, M. P. Nash, D. Chapelle, D. A. Nordsletten, and L. Mall. Multiphysics and multiscale modelling , data—-model fusion and integration of organ physiology in the clinic : ventricular cardiac mechanics. *Interface Focus*, 2016. https://doi.org/10.1098/rsfs.2015.0083.

[11]Clay, S., K. Alfakih, A. Radjenovic, T. Jones, J. P. Ridgway, and M. U. Sinvananthan. Normal range of human left ventricular volumes and mass using steady state free precession MRI in the radial long axis orientation. *Mag. Resonance Mater. Phys. Biol. Med.* 19(1), 41–45, 2006.

[12]CMRG. Continuity 6.4, 2015.

[13]Ellwein, L. M., S. R. Pope, A. Xie, J. Batzel, C. T. Kelley, and M. S. Olufsen. Modeling cardiovascular and respiratory dynamics in congestive heart failure. *Math. Biosci.* 241:56–74, 2013.

[14]Ennis, D. B. Assessment of Myocardial Structure and Function Using Magnetic Resonance Imaging. PhD thesis, Johns Hopkins University, 2004.

[15]Hadjicharalambous, M., L. Asner, R. Chabiniok, E. Sammut, J. Wong, D. Peressutti, E. Kerfoot, A. King, J. Lee, R. Razavi, N. Smith, G. Carr-White, and D. Nordsletten. Non-invasive model-based assessment of passive left-ventricular myocardial stiffness in healthy subjects and in patients with non-ischemic dilated cardiomyopathy. *Ann. Biomed. Eng.* 45(3): 605–618, 2017.

[16]Heusinkveld, M., K. Reesink, T. Arts, W. Huberts, and T. Delhaas. Use of vascular adaptation in response to mechanical loading facilitates personalisation of a one-dimensional pulse wave propagation model. *Artery Res.* 20:79–80, 2009.

[17]Holzapfel, G. A., and R. W. Ogden Constitutive modelling of passive myocardium: a structurally based framework for material characterization. *Philos. Trans. R. Soc. Ser. A* 367(1902):3445–3475, 2009.

[18]Hooke, R., and T. A. Jeeves. "Direct search" solution of numerical and statistical problems. *J. ACM* 8(2):212–229, 1961.

[19]Institute of Laboratory Animal Resources (ILAR). Guide for the Care and Use of Laboratory Animals. Washington, D.C.: National Academies Press, 1996.

[20]Kerckhoffs, R. C. P., J. Lumens, K. Vernooy, J. H. Omens, L. J. Mulligan, T. Delhaas, T. Arts, A. D. McCulloch, and F. W. Prinzen. Cardiac resynchronization: insight from experimental and computational models. *Prog. Biophys. Mol. Biol.* 97(2–3), 543–561, 2008.

[21]Klotz, S., I. Hay, M. L. Dickstein, G. H. Yi, J. Wang, M. S. Maurer, D. A. Kass, and D. Burkhoff. Single-beat estimation of end-diastolic pressure-volume relationship: a novel method with potential for noninvasive application. *Am. J. Physiol.* 291(1):H403–H412, 2006.

[22]Kovalova, S., J. Necas, and J. Vespalec. What is a "normal" right ventricle? *Eur. J. Echocardiogr.* 7(4):293–297, 2006.

[23]Krishnamurthy, A., B. Coppola, J. Tangney, R. C. P. Kerckhoffs, J. H. Omens, and A. D. McCulloch. A microstructurally based multi-scale constitutive model of active myocardial mechanics. In: Structure-Based Mechanics of Tissues and Organs. New York: Springer, chap 3, pp. 439–460, 2016.

[24]Krishnamurthy, A., C. Villingco, A. Beck, J. Omens, and A. McCulloch. Left ventricular diastolic and systolic material property estimation from image data: LV mechanics challenge. *Stat. Atlases Comput. Model. Heart* 8896:63–73, 2015.

[25]Krishnamurthy, A., C. T. Villongco, J. Chuang, L. R. Frank, V. Nigam, E. Belezzuoli, P. Stark, D. E. Krummen, S. Narayan, J. H. Omens, A. D. McCulloch, R. C. P. Kerckhoffs. Patient-specific models of cardiac biomechanics. J. Comput. Phys. 244:4–21, 2013.

[26]Lang, R. M., M. Bierig, R. B. Devereux, F. A. Flachskampf, E. Foster, P. A. Pellikka, M. H. Picard, M. J. Roman, J. Seward, J. Shanewise, S. Solomon, K. T. Spencer, M. St John Sutton, and W. Stewart. Recommendations for chamber quantification. *Eur. J. Echocardiogr.* 7(2):79–108, 2006.

[27]Lim, E., S. Dokos, N. H. Lovell, S. L. Cloherty, R. F. Salamonsen, D. G. Mason, and J. A. Reizes. Parameter-optimized model of cardiovascular-rotary blood pump interactions. *IEEE Trans. Biomed. Eng.* 57(2):254–266, 2010.

[28]Marchesseau, S., H. Delingette, M. Sermesant, and N. Ayache. Fast parameter calibration of a cardiac electromechanical model from medical images based on the unscented transform. *Biomech. Model. Mechanobiol.* 12(4), 815–831, 2013.

[29]MathWorks. MATLAB R2017b, 2017.

[30]More, J. J., and S. M. Wild. Benchmarking derivative-free optimization algorithms. *SIAM J. Optim.* 39:2, 2009.

[31]Nasopoulou, A., A. Shetty, J. Lee, D. Nordsletten, C. A. Rinaldi, P. Lamata, and S. Niederer. Improved identifiability of myocardial material parameters by an energy-based cost function. *Biomech. Model. Mechanobiol.* 16(3), 971–988, 2017.
[32]Nauser, T. D., and S. W. Stites. Diagnosis and treatment of pulmonary hypertension. *Am. Family Phys.* 63(9):1789–1798, 2001.
[33]Neal, M. L., and J. B. Bassingthwaighte. Subject-specific model estimation of cardiac output and blood volume during hemorrhage. *Cardiovasc. Eng.* 7(3):97–120, 2007.
[34]Niederer, S. A., M. Fink, D. Noble, and N. P. Smith. A meta-analysis of cardiac electrophysiology computational models. *Exp. Physiol.* 94(5):486–495, 2009.
[35]Piper, M. A., C. V. Evans, B. U. Burda, K. L. Margolis, E. O'Connor, and E. P. Whitlock. Diagnostic and predictive accuracy of blood pressure screening methods with consideration of rescreening intervals: a systematic review for the U.S. Preventive Services Task Force. *Ann. Int. Med.* 162(3):192–204, 2015.
[36]Raamat, R., J. Talts, K. Jagomägi, and J. Kivastik. Accuracy of some algorithms to determine the oscillometric mean arterial pressure: a theoretical study. *Blood Press. Monit.* 18:50–56, 2013.
[37]Sellier, M. An iterative method for the inverse elasto-static problem. *J. Fluid. Struct.* 27(8):1461–1470, 2011.
[38]Shi, Y., and R. Eberhart. A modified particle swarm optimizer. In: IEEE International Conference on Evolutionary Computation, pp. 69–73, 1998.
[39]Shortliffe, E. H., B. G. Buchanan, and E. A. Feigenbaum. Knowledge engineering for medical decision making: a review of computer-based clinical decision aids. Tech. Rep., Stanford University Computer Science Department, 1979.
[40]Tange, O. GNU parallel—the command-line power tool. *login USENIX Mag.* 36(1):42–47, 2011.
[41]Vaz, A. I. F., and L. N. Vicente. A particle swarm pattern search method for bound constrained global optimization. *J. Glob. Optim.* 39(2):197–219, 2007.
[42]Wang, V. Y., H. I. Lam, D. B. Ennis, B. R. Cowan, A. A. Young, and M. P. Nash. Modelling passive diastolic mechanics with quantitative MRI of cardiac structure and function. *Med. Image Anal.* 13(5):773–784, 2009.
[43]Wang, V. Y., P. M. F. Nielsen, and M. P. Nash. Image-based predictive modeling of heart mechanics. *Ann. Rev. Biomed. Eng.* 17:351–383, 2015.
[44]Xi, J., P. Lamata, S. Niederer, S. Land, W. Shi, X. Zhuang, S. Ourselin, S. G. Duckett, A. K. Shetty, C. A. Rinaldi, D. Rueckert, R. Razavi, and N. P. Smith. The estimation of patient-specific cardiac diastolic functions from clinical measurements. *Med. Image Anal.* 17(2):133–146, 2013.
[45]Yoshimura, M., H. Yasue, K. Okumura, H. Ogawa, M. Jougasaki, M. Mukoyama, K. Nakao, and H. Imura. Different secretion patterns of atrial natriuretic peptide and brain natriuretic peptide in patients with congestive heart failure. *Circulation* 87(2):464–469, 1993.
[46]Zoghbi, W. A. Quantifying valvular regurgitation. In: ACC Middle East Conference, 2016.